Food and Chemical Toxicology 116 (2018) 161–172

Contents lists available at ScienceDirect

Food and Chemical Toxicology

journal homepage: www.elsevier.com/locate/foodchemtox

Silibinin is a direct inhibitor of STAT3

Sara Verdura[a,b,1], Elisabet Cuyàs[a,b,1], Laura Llorach-Parés[c], Almudena Pérez-Sánchez[d], Vicente Micol[d,e], Alfons Nonell-Canals[c], Jorge Joven[f], Manuel Valiente[g], Melchor Sánchez-Martínez[c], Joaquim Bosch-Barrera[h,i,**], Javier A. Menendez[a,b,*]

[a] Program Against Cancer Therapeutic Resistance (ProCURE), Metabolism and Cancer Group, Catalan Institute of Oncology, Girona, Spain
[b] Molecular Oncology Group, Girona Biomedical Research Institute (IDIBGI), Girona, Spain
[c] Mind the Byte, Barcelona, Spain
[d] Instituto de Biología Molecular y Celular (IBMC), Miguel Hernández University (UMH), Elche, Alicante, Spain
[e] CIBER, Fisiopatología de la Obesidad y la Nutrición, CIBERobn, Instituto de Salud Carlos III (CB12/03/30038), Spain
[f] Unitat de Recerca Biomèdica, Hospital Universitari de Sant Joan, IISPV, Rovira i Virgili University, Reus, Spain
[g] Brain Metastasis Group, Molecular Oncology Program, Spanish National Cancer Research Centre (CNIO), Madrid, Spain
[h] Department of Medical Oncology, Catalan Institute of Oncology, Girona, Spain
[i] Department of Medical Sciences, Medical School, University of Girona, Girona, Spain

ARTICLE INFO

Keywords:
Silibinin
STAT3
Cancer
Metastasis

ABSTRACT

We herein combined experimental and computational efforts to delineate the mechanism of action through which the flavonolignan silibinin targets STAT3. Silibinin reduced IL-6 inducible, constitutive, and acquired feedback activation of STAT3 at tyrosine 705 (Y705). Silibinin attenuated the inducible phospho-activation of Y705 in GFP-STAT3 genetic fusions without drastically altering the kinase activity of the STAT3 upstream kinases JAK1 and JAK2. A comparative computational study based on docking and molecular dynamics simulation over 14 different STAT3 inhibitors (STAT3i) predicted that silibinin could directly bind with high affinity to both the Src homology-2 (SH2) domain and the DNA-binding domain (DBD) of STAT3. Silibinin partially overlapped with the cavity occupied by other STAT3i in the SH2 domain to indirectly prevent Y705 phosphorylation, yet showing a unique binding mode. Moreover, silibinin was the only STAT3i predicted to establish direct interactions with DNA in its targeting to the STAT3 DBD. The prevention of STAT3 nuclear translocation, the blockade of the binding of activated STAT3 to its consensus DNA sequence, and the suppression of STAT3-directed transcriptional activity confirmed silibinin as a direct STAT3i. The unique characteristics of silibinin as a bimodal SH2- and DBD-targeting STAT3i make silibinin a promising lead for designing new, more effective STAT3i.

1. Introduction

The aberrant activation of signal transducer and activator of transcription 3 (STAT3) contributes to cancer initiation and progression in a multi-faceted manner via promotion of cell proliferation/survival, invasion/migration, angiogenesis, and immune-evasion (Chang et al., 2013; Sansone and Bromberg, 2012; Yu et al., 2009, 2014). Feedback activation of STAT3 additionally mediates tumor resistance to a broad spectrum of cancer therapies, including radiotherapy, conventional chemotherapy, and modern targeted therapies (Lee et al., 2014; Poli and Camporeale, 2015; Tan et al., 2014; Zhao et al., 2016). STAT3 activation associates also with the generation and maintenance of cancer stem cells (CSC), a particularly aggressive type of malignant cell defined in terms of functional traits including tumor/metastasis-initiating capacity and therapy resistance (Kroon et al., 2013; Misra et al., 2018; Schroeder et al., 2014; Wang et al., 2018). Not surprisingly, the activation status of STAT3 is a strong predictor of poor prognosis and is an independent risk factor for tumor recurrence and post-therapy progression (Chen et al., 2013; Liu et al., 2012; Tong et al., 2017; Wu et al., 2016). These observations have motivated great efforts over the last decade to clinically exploit the beneficial effects of inhibiting STAT3 in human malignancies. Accordingly, a large number of STAT3 inhibitors (STAT3i) have been developed as potential cancer therapeutics (Fagard et al., 2013; Furtek et al., 2016a; b; Jin et al., 2016; Miklossy et al.,

* Corresponding author. Catalan Institute of Oncology (ICO), Girona Biomedical Research Institute (IDIBGI), Edifici M2, Parc Hospitalari Martí i Julià, E-17190 Salt, Girona, Spain.
** Corresponding author. Catalan Institute of Oncology (ICO), Hospital Dr. Josep Trueta de Girona, Avda. de França s/n, 17007, Girona, Spain
E-mail addresses: jbosch@iconcologia.net (J. Bosch-Barrera), jmenendez@iconcologia.net, jmenendez@idibgi.org (J.A. Menendez).
[1] These authors contributed equally.

https://doi.org/10.1016/j.fct.2018.04.028
Received 8 March 2018; Received in revised form 3 April 2018; Accepted 13 April 2018
Available online 14 April 2018
0278-6915/

2013; Siveen et al., 2014; Yue and Turkson, 2009).

STAT3i can be classified as indirect or direct according to their mode of action. Indirect STAT3i interfere with cytokine- and growth factor receptor-activated upstream kinases such as the Janus kinases (JAK) that phosphorylate STAT3. Direct STAT3i bind to STAT3 protein domains critically involved in STAT3 activation/dimerization (Src homology 2 domain, SH2) or DNA binding (DNA-binding domain, DBD). The usage of broad-spectrum indirect STAT3i (e.g., JAK inhibitors), however, often results in undesirable off-target effects. Research into direct STAT3i has focused mainly on targeting the SH2 domain, the protein-protein interface responsible for the formation of STAT3 dimers by reciprocal phosphotyrosine-SH2 interactions following activation of the tyrosine 705 (Y705) residue. Unfortunately, only a limited number of direct, SH2-targeted STAT3i have reached preclinical and clinical trials. This is due mostly to the intrinsic difficulty in developing small molecules capable of efficaciously disrupting protein-protein interactions over a large surface such as those involving SH2-mediated STAT3 dimerization, while maintaining drug-like properties *in vivo*. Moreover, the sole blockade of active STAT3 dimers might not be sufficient to fully abrogate STAT3 signaling (Nkansah et al., 2013; Timofeeva et al., 2012). Although targeting of the STAT3 DBD and disruption of its DNA binding activity has the potential to circumvent the transcriptional activation of STAT3 irrespective of its activation/dimerization status (Huang et al., 2016), very few small molecules have been reported to date as STAT3 DBD inhibitors. This is mainly due to the previously thought undruggable nature of the DBD and potentially limited selectivity (Huang et al., 2016), and also the lack of adequate assay systems (Furtek et al., 2016a; b). Furthermore, there are only three crystal structures available [PDB ID: 4E68 (Nkansah et al., 2013), 3CWG (Ren et al., 2008), and 1BG1 (Becker et al., 1998)] of the mouse but not human core STAT3 fragment containing the SH2 and DBD domains in the Protein Data Bank (http://www.rcsb.org), and co-crystal structures of STAT3i bound to STAT3 are lacking.

There is ever-growing evidence that the flavonolignan silibinin, the major bioactive constituent of the seed extract of the plant Milk thistle (*Silybum marianum*) (Agarwal et al., 2006; Cufí et al., 2013a,b; Gažák et al., 2007), possesses drug-like properties with proven clinical activity via inhibition of STAT3 signaling (Chittezhath et al., 2008; Cuyàs et al., 2016; Shukla et al., 2015; Singh et al., 2009). Although initial clinical experiences with silibinin supplementation in cancer patients have been disappointing (Flaig et al., 2010; Hoh et al., 2006; Siegel et al., 2014), new silibinin formulations with improved water solubility, absorption, and bioavailability appear to translate into proven therapeutic benefits (Bosch-Barrera et al., 2014, 2016). Unfortunately, whereas the possibility of providing oncologists with new silibinin formulations or silibinin derivatives capable of functioning as STAT3i in a clinical setting may broaden their therapeutic armamentarium (Bosch-Barrera and Menendez, 2015; Bosch-Barrera et al., 2017), the precise mechanism through which silibinin targets STAT3 remains unknown. Here, we aimed to combine experimental and *in silico* efforts to clearly delineate the molecular bases of the silibinin-STAT3 interaction.

2. Materials and methods

2.1. Reagents

Recombinant IL-6 (Cat. No. 7270-IL-25) was obtained from R&D. ONE-Glo™ Luciferase Assay System (Cat. No E6110) and the pGL4.47 (luc2P/STAT-3 inducible element [SIE]/Hygro) vector (Cat. No E4041) were purchased from Promega (Madison, WI, USA). TransAM® Transcription Factor ELISA (Cat. No 45196) was obtained from Active Motif (Carlsbad, CA, USA). Antibodies against total STAT3 (124H6, Cat. No 9139) and phospho-STAT3 Tyr705 (D3A7, Cat. No 9145S) were purchased from Cell Signaling Technology (Beverly, MA, USA). H2228 and H2228/CR cells were generously provided by Daniel B. Costa (Division of Hematology/Oncology, Beth Israel Deaconess Medical Center, Boston, USA).

2.2. LanthaScreen STAT3 GripTite inhibitor screen

To characterize the STAT3 inhibitory potency of silibinin, IC_{50} determinations for phospho-$STAT3^{Y705}$ were outsourced to Invitrogen (Life Technologies) using the LanthaScreen STAT3 GripTite inhibitor screen service. Briefly, cells were thawed and resuspended in Assay Medium (OPTI-MEM, 1% csFBS, 0.1 mmoL/L NEAA, 1 mmoL/L sodium pyruvate, 100 U/mL/100 µg/mL Pen/Strep) to a concentration of 625,000 cells/mL. Thirty-two microliters of the cell suspension were added to each well of a white tissue culture-treated assay plate (20,000 cells/well) and incubated for 16–26 h at 37 °C/5% CO_2 in a humidified incubator. Then, 4 µL of the control inhibitor JAK Inhibitor I or silibinin was added to the appropriate assay wells followed by the addition of 4 µL of Assay Medium. The assay plate was incubated for 30–60 min at 37 °C/5% CO_2 in a humidified incubator. Then 4 µL of a 10 × control activator, IFN-α or IL-6 at the pre-determined EC_{80} concentration, was added to wells containing the control inhibitor or silibinin. The assay plate was then incubated as before for 30 min. Next, the assay medium was aspirated from the wells and 20 µL of LanthaScreen Cellular Assay Lysis Buffer containing 5 nmoL/L of LanthaScreen Tb-anti-$STAT3^{Y705}$ antibody was added. The assay plate was incubated for 60 min at room temperature and then read with a fluorescent plate reader.

2.3. Z′-LYTE JAK kinase activity assay

To characterize the JAK1/JAK2 kinase inhibitory potency of silibinin, IC_{50} determinations for JAK1/JAK2 kinase activity were outsourced to Invitrogen (Life Technologies) using the FRET-based Z-LYTE™ SelectScreen Kinase Profiling Service. The 2 × JAK1/Tyr 06 or JAK2/Tyr 06 mixture was prepared in 50 mmoL/L HEPES pH 6.5, 0.01% BRIJ-35, 10 mmoL/L MgCl2, 1 mmoL/L EGTA, and 0.02% NaN_3. The final 10 µL Kinase Reaction consisted of 21.2–91.5 ng JAK1 (or JAK2) and 2 µmoL/L Tyr 06 in 50 mmoL/L HEPES pH 7.0, 0.01% BRIJ-35, 10 mmoL/L $MgCl_2$, 1 mmoL/L EGTA, and 0.01% NaN_3. After incubation for 1 h, 5 µL of a 1:128 dilution of Development Reagent A was added.

SelectScreen Kinase Profiling Service uses XLfit software from ID Business Solutions (UK). The dose response curve is fitted to model number 205 (sigmoidal dose-response model). If the bottom of the curve does not fit between −20% and 20% inhibition, it is set to 0% inhibition. If the top of the curve does not fit between 70% and 130% inhibition, it is set to 100% inhibition.

2.4. Computational modeling of human STAT3

The homology-modeling software tools SWISS-MODEL and I-TASSER were employed to generate a computational homology model of human STAT3. The human amino acidic sequence [UniprotID P40763] was extracted from Uniprotkb and, in both cases, the three-dimensional crystal structure of the mouse STAT3 homodimer bound to DNA [PDB ID 1BG1 (Becker et al., 1998)] was employed as template. Whereas SWISS-MODEL generated a homology model that failed to cover a few residues on the SH2 domain, I-TASSER employed 1BG1 and other templates including 4E68 (unphosphorylated mouse STAT3 core protein binding to double-stranded DNA (Nkansah et al., 2013)), 3CWG (unphosphorylated mouse STAT3 core fragment (Ren et al., 2008)), and 1YVL (unphosphorylated mouse STAT1 (Mao et al., 2005)) to cover a larger extent of the protein. All the PDB entries used to generate structures were constructed as monomers and then assembled as dimers using 1BG1 as template.

2.5. Docking calculations

All docking calculations were performed using Itzamna and Kin (www.mindthebyte.com), classical docking, and blind-docking software tools. Protein structures from RSCB PDB as well as the above-mentioned human homology models were directly employed for docking calculations using the SH2 and DBD cavities defined in the literature as STAT3 binding regions. Two runs were carried out for each calculation to avoid false positives.

2.6. Molecular dynamics (MD) simulations

Docking post-processing allowing conformational selections/induced fit events to optimize the interactions were performed via short (1 ns) MD simulations using NAMD version 2.10 over the best-docked complexes, which were selected based on the interaction energy. The Ambers99SB-ILDN and the GAFF forcefield set of parameters were employed for STAT3 and STAT3i including silibinin, respectively. The GAFF parameters were obtained using Acpype software, whereas the STAT3 structures were modeled using the leap module of Amber Tools. Simulations were carried out in explicit solvent using the TIP3P water model with the imposition of periodic boundary conditions *via* a cubic box. Electrostatic interactions were calculated by the particle-mesh Ewald method using constant pressure and temperature conditions. Each complex was solvated with a minimum distance of 10 Å from the surface of the complex to the edge of the simulation box. Na^+ or Cl^- ions were also added to the simulation to neutralize the overall charge of the systems. The temperature was maintained at 300 K using a Langevin thermostat, and the pressure was maintained at 1 atm using a Langevin Piston barostat. The time step employed was 2 fs. Bond lengths to hydrogens were constrained with the SHAKE algorithm. Before production runs, the structure was energy minimized followed by a slow heating-up phase using harmonic position restraints on the heavy atoms of the protein. Subsequently, the system was energy minimized until volume equilibration, followed by the production run without any position restraints.

2.7. Binding free energy analysis

Molecular Mechanics/Generalized Borne Surface Area (MM/GBSA) calculations were performed to calculate the alchemical binding free energy (ΔG_{bind}) of silibinin and direct STAT3i against STAT3. MM/GBSA rescoring was performed using the MMPBSA.py algorithm within AmberTools. The snapshots generated in the 1 ns MD simulation were imputed into the post-simulation MM/GBSA calculations of binding free energy. Graphical representations were prepared using PyMOL program and PLIP version 1.3.0.

2.8. Interaction analysis

The predicted binding site residues of silibinin to the SH2 and DBD domains of STAT3 were defined using evidence-based interaction analyses of known STAT3 inhibitors with well-defined binding residues in the SH2 and DBS sites.

2.9. Indirect immunofluorescence microscopy

Cells seeded on a glass plate were fixed with methanol and incubated with the respective antibodies against STAT3 and phospho-STAT3 Tyr705. Antibody binding was localized with either a goat anti-rabbit IgG (H + L) secondary antibody, Alexa Fluor® 594 conjugate or a goat anti-mouse IgG (H + L) secondary antibody, Alexa Fluor® 488 conjugate (both from Invitrogen). Nuclei were counterstained with Hoechst 33342. Images were obtained with a Nikon Eclipse 50i fluorescence microscope including NIS-Elements imaging software.

2.10. STAT3 luciferase reporter assay

Luciferase activities of HEK293T cells transfected with the pGL4.47 reporter, in which five copies of the STAT3 DNA binding site-containing the SIE drives transcription of the luciferase-reporter gene luc2P (Photinus pyralis, 2), were measured using a Dual-Luciferase Reporter Assay System (ONE-Glo™, Promega).

2.11. STAT3 TransAM™ enzyme-linked immunosorbent assay

The STAT3 DNA-binding assay was performed using the TransAM™ Transcription Factor ELISA. Briefly, nuclear extracts from IL-6-stimulated cells containing activated STAT3 were directly added with graded concentrations of silibinin and complete binding buffer to microtiter wells coated with the STAT3 consensus sequence (5′-TTCCCGGAA-3′) for 3 h at room temperature. The wells were washed three times with 1 × wash buffer, and incubated with STAT3 antibody for 1 h. The wells were then washed as before and incubated with a horseradish peroxide-conjugated secondary antibody at room temperature for 1 h. After washing again, 100 µL of developing solution was added to the wells, which was quenched with 100 µL of stop solution, and the absorbance was measured at 450 nm.

2.12. Statistical analysis

All statistical analyses were performed using XLSTAT 2010 (Addinsoft™). For all experiments, at least three independent biological replicates were performed with $n \geq 3$ technical replicates per experiment. No statistical method was used to predetermine sample size. Investigators were not blinded to data allocation. Experiments were not randomized. Data are presented as mean ± S.D. Two-group comparisons were performed using Student's *t*-test for paired and unpaired values. Comparisons of means of ≥3 groups were performed by ANOVA, and the existence of individual differences, in case of significant *F* values at ANOVA, were tested by Scheffé's multiple contrasts. *P* values < 0.05 were considered to be statistically significant (denoted as *). All statistical tests were two-sided.

3. Results

3.1. Silibinin inhibits Y705 STAT3 phosphorylation in cell-based assays

We initially assessed the ability of silibinin to interfere with the three known activating modes of Y705 STAT3 phosphorylation, namely IL-6-inducible, constitutive, and acquired (feedback hyperactivation), in a panel of non-small cell lung carcinoma (NSCLC) cell lines (Fig. 1A). H460 and PC9 cell lines, which do not express persistently hyperphosphorylated STAT3, were used to determine whether silibinin could inhibit Y705 STAT3 phosphorylation induced by the pro-inflammatory cytokine IL-6. Immunoblotting procedures revealed that silibinin treatment completely prevented the capacity of IL-6 to induce the phosphorylation of Y705 STAT3 in H460 cells (Fig. 1B). Moreover, the ability of IL-6 to augment by 4.0-fold the phosphorylation of Y705 STAT3 in PC9 cells was reduced to 2.1-fold in the presence of silibinin (Fig. 1B). This prevention of IL-6-inducible Y705 STAT3 phosphorylation was accompanied by a rapid and noteworthy reduction in the protein level of the key STAT3 target gene c-MYC in H460 and PC9 cells (Fig. 1B).

Treatment with graded concentrations of silibinin dose-dependently abrogated Y705 STAT3 phosphorylation in the H2228 cell line, which exhibits constitutive hyperphosphorylation of STAT3 (Fig. 1C). Silibinin also suppressed, in a dose-dependent manner, the acquired feedback hyperactivation of Y705 STAT3 in H3122CR cells, which has been shown to occur as a non-genetic mechanism of acquired resistance to the ALK-tyrosine kinase inhibitor crizotinib in ALK-rearranged H3122 parental cells (Cuyàs et al., 2016) (Fig. 1D).

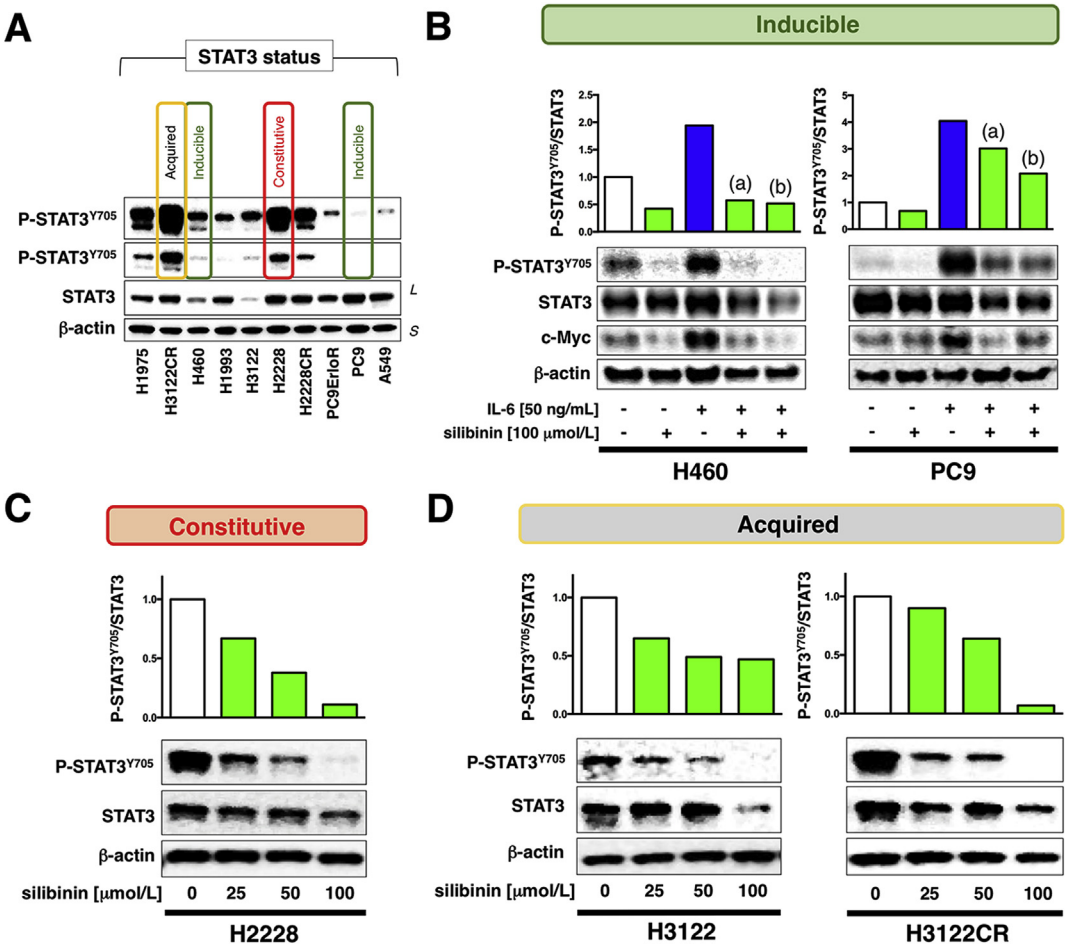

Fig. 1. Silibinin inhibits phosphorylation of STAT3 Y705. A. Baseline levels of STAT3 and P-STAT3^{Tyr705} in various NSCLC cell lines were detected by immunoblotting using specific antibodies (S: short exposure; L: long exposure) **B.** Silibinin inhibits STAT3 Y705 phosphorylation induced by IL-6. H460 and PC-9 cells were serum-starved overnight, and then left untreated or treated with 100 μmoL/L silibinin. After 3 h, the untreated and silibinin-treated cells were stimulated with IL-6 for 1 h to induce phosphorylated Y705 STAT3 (a). Alternatively, overnight serum-starved cells were left untreated or stimulated with IL-6. After 1 h, the untreated and IL-6-stimulated cells were treated with silibinin for 3 h (b). **C.** Silibinin inhibits constitutively active STAT3 Y705 phosphorylation. H2228 cells were serum-starved overnight and treated with graded concentrations of silibinin (0, 25, 50, and 100 μmoL/L) for 48 h. **D.** Silibinin inhibits acquired phospho-activation of STAT3 at Y705. Crizotinib-responsible H2228 cells (low phospho-STAT3^{Y705} at baseline) and crizotinib-resistant H2228/CR derivatives (high, acquired phospho-STAT^{Y705}) were serum-starved overnight and treated with graded concentrations of silibinin (0, 25, 50, and 100 μmoL/L) for 48 h. Figures show representative immunoblots and densitometric analyses of multiple ($n = 3$) independent experiments.

3.2. Silibinin inhibits Y705 STAT3 phosphorylation in a JAK1/JAK2-independent manner

We used the LanthaScreen® STAT3 GripTite™ HEK293 human cell line that constitutively expresses a GFP-STAT3 fusion protein to confirm the STAT3 inhibitory activity of silibinin. Because the activation state of the tyrosine kinases JAK1 and JAK2 is considered to be the main effector mechanism for Y705 STAT3 phosphorylation (Chang et al., 2013; Sansone and Bromberg, 2012; Yu et al., 2009), and given that the JAK/STAT3 signaling pathway is functionally intact in the STAT3 GripTite™ cell line, the GFP-STAT3 fusion protein serves as a direct substrate for assessing IL-6- and IFN-α-inducible STAT3 phosphorylation. We pre-incubated serum-starved STAT3 GripTite™ HEK293 cells with graded concentrations of silibinin for 1 h prior to stimulation with IL-6 or IFN-α (for 30 min) at the pre-determined EC_{80} effective concentration for optimized JAK-mediated GFP-STAT3 phosphorylation. A lytic immunoassay was then developed in which the phosphorylation state of GFP-STAT3 was detected in cell lysates using a terbium-labeled anti-pY705-STAT3 antibody in a time-resolved FRET (TR-FRET) readout (Supplementary Fig. S1A). The IL-6 stimulation/silibinin inhibitor screen provided a Z′ factor of 0.74, which indicated good signal separation and plate uniformity, whereas the IFN-α stimulation/silibinin inhibitor screen provided a Z' factor of 0.57, which was acceptable by high-throughput screening standards. Both assays showed a dose-dependent decrease in the TR-FRET signals with IC_{50} values of 320 μmoL/L for IL-6-stimulated phosphorylation of Y705 STAT3 and 182 μmoL/L for IFN-α-stimulated phosphorylation of Y705 STAT3 (Fig. 2A). We then used the FRET-based Z-LYTE™Kinase Assay to detect and characterize the ability of silibinin to directly operate as a JAK1/JAK2 kinase inhibitor (Supplementary Fig. S1B). When ten concentrations of silibinin over five logarithmic decades were selected, we failed to detect any significant inhibitory activity of silibinin towards the kinase activity of JAK1 and JAK2 (Fig. 2B).

3.3. Generation of a computational homology model of the human STAT3 protein: A comparative study of silibinin and multiple STAT3i

To test whether the inhibitory mode of action of silibinin against STAT3 might involve its direct binding to the STAT3 protein, we generated a computational homology model of human STAT3 protein (see the *Material and methods* section for details).

Fig. 3A depicts all the STAT3i included in our comparative *in silico* analysis of the binding of silibinin to STAT3, including Stattic (Schust et al., 2006), S31-M2011 (Furqan et al., 2013), TPCA-1 (Nan et al.,

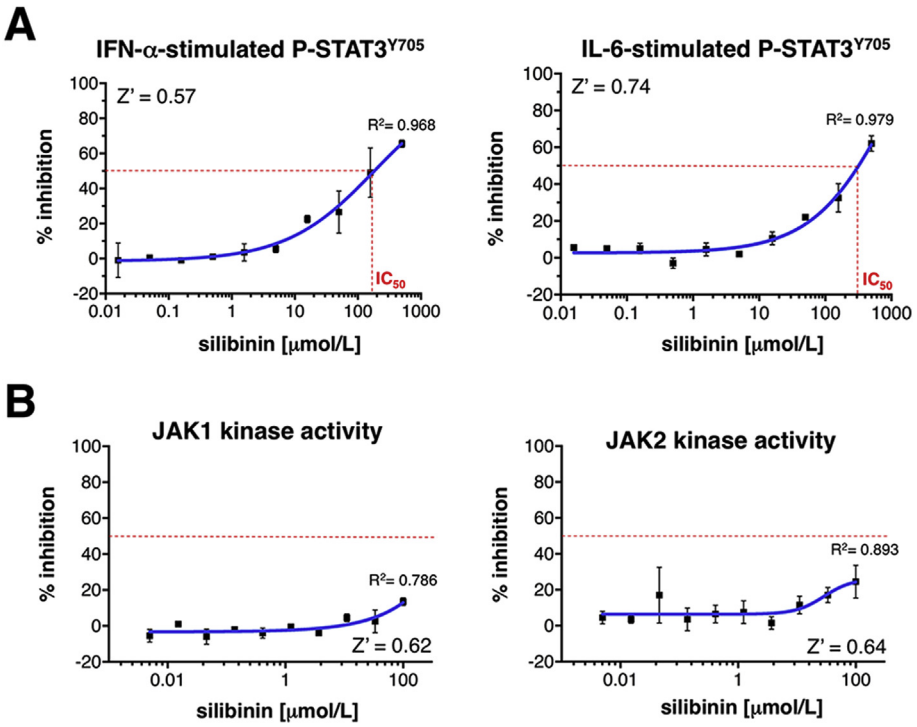

Fig. 2. Silibinin inhibits phospho-activation of STAT3 without targeting the STAT3 kinase JAK1/JAK2. A. Graphs shows the 520/490 nm emission ratios of silibinin-treated LanthaScreen® STAT3 GripTite™ cells (one representative experiment carried out in triplicate). **B.** Figure shows dose-response curves of ATP-dependent JAK1/JAK2 kinase activities for one representative experiment carried out in triplicate, created by plotting FRET signal of the Z′-LYTE Kinase assay as the function of silibinin concentration. See Supplementary Figs. S1A and B for schematic description of details concerning LanthaScreen® and Z′-LYTE assays.

2014), OPB-31121 (Brambilla et al., 2015), LLL-12 (Lin et al., 2010), lnS3-54A18 (Zhao et al., 2016), HO-3687 (Rath et al., 2014), BP5-087 (Eiring et al., 2015), STX-0119 (Matsuno et al., 2010), ISS610 (Shahani et al., 2011), SH-4-054 (Ali et al., 2016), S31-1757 (Zhang et al., 2013), Compound 50 (Lai et al., 2015), and Compound 24 (Lai et al., 2015). When classical docking calculations were performed against cavities of both the SH2 domain and the DBD (Fig. 3B–D), we observed that all the STAT3i as well as silibinin were placed in the middle of the corresponding regions of each domain by sharing residues between both chains. Although this behavior reproduced a plausible binding mode capable of disrupting the STAT3 dimer, as previously reported for some STAT3i, it is acknowledged that the majority of STAT3i have been

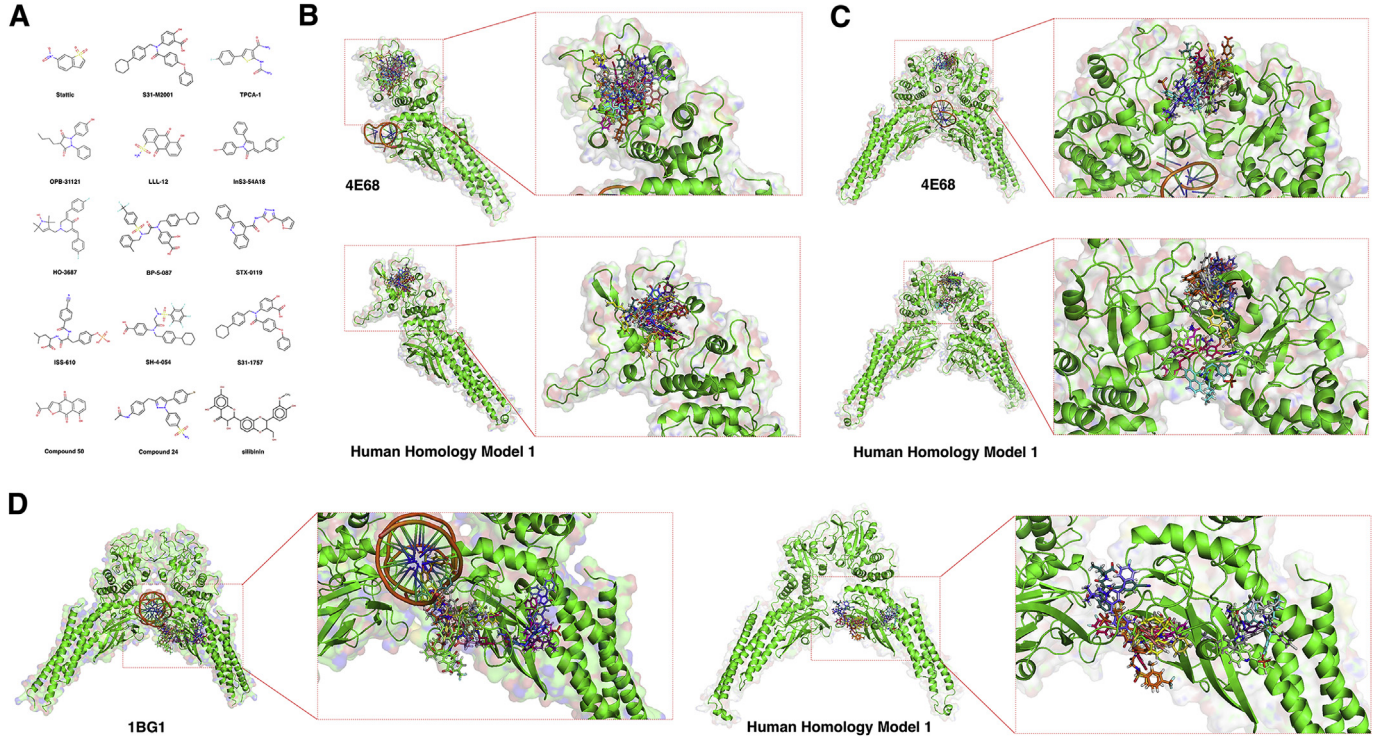

Fig. 3. Silibinin is computationally predicted to behave as a direct STAT3i. A. Chemical structures of the direct STAT3i included in a comparative computational study of silibinin as a direct STAT3i. **B**, **C**, and **D**. Overall structures and views of the interactions between direct STAT3i with the monomeric SH2 binding region (**A**), the binding region between SH2 dimers (**B**), and the DBD domain at STAT3 DBD domain-DNA complex (**C**) assembled from PDBIDs 4E68 and 1BG1, or human homology model 1, as specified.

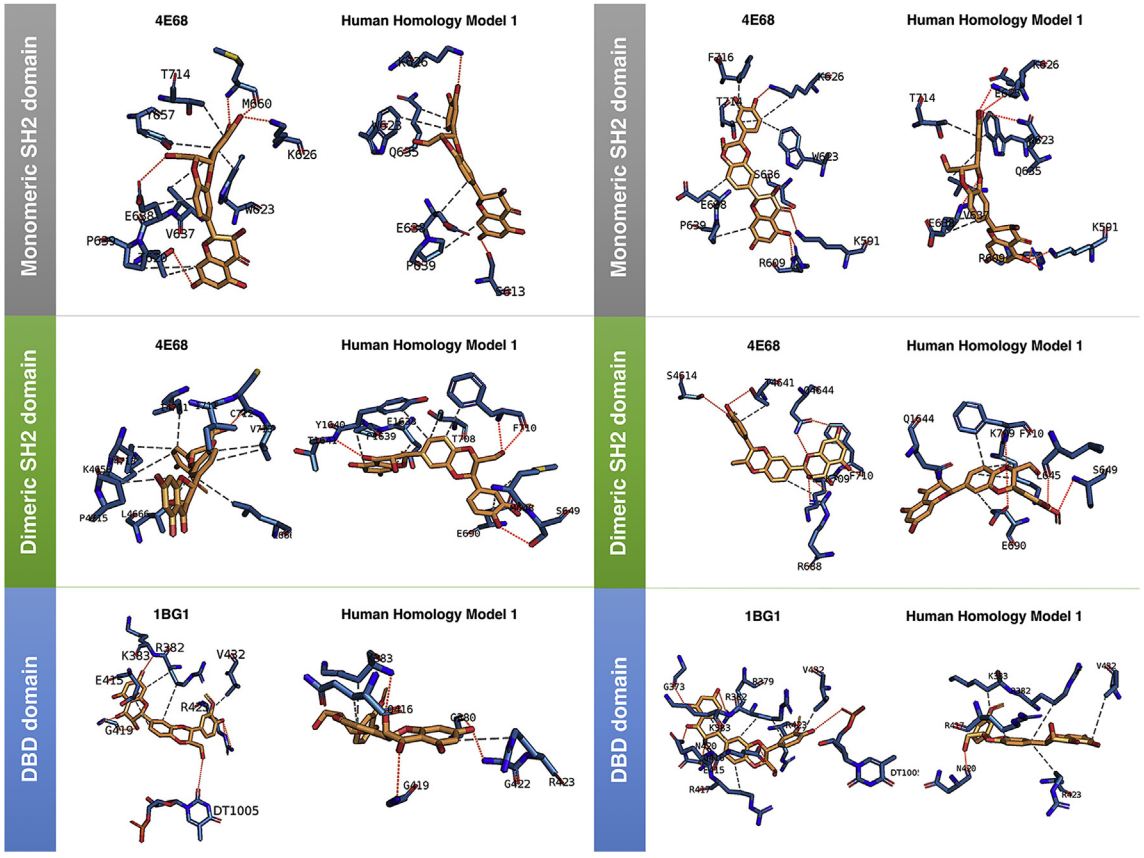

Fig. 4. Mode of binding of silibinin to SH2 activation/dimerization and DNA binding (DBD) domains of STAT3. Figure shows in sticks all the pharmacophoric interaction residues involved in the *in silico* binding of silibinin to the SH2 and DBD domains of STAT3, using PLIP. Orange dashed lines represent hydrogen bond interactions; grey dashed lines represent hydrophobic interactions. The main residues involved in silibinin interaction with the protein backbone are shown in black; the residue numbers shown correspond to the original PDB file numbering. *Left panels* correspond to binding poses resulting from simple, rigid docking studies; *right panels* correspond to self-docking poses under molecular dynamics (MD) simulations modeling the backbone and ligand (silibinin) flexibility. (For interpretation of the references to colour in this figure legend, the reader is referred to the Web version of this article.)

suggested to bind the corresponding SH2 or DBD domain solely in one of the monomers, without sharing residues with the other one. To explore in more detail the latter behavior, we performed docking simulations to the monomeric structures, to mimic the desired binding of known STAT3i. The binding energies obtained from *in silico* binding experiments using rigid docking calculations, which were run twice to avoid false positives, are summarized in Table S1 (SH2 domain of monomeric structures), Table S2 (SH2 domain of dimeric structures), and Table S3 (DBD of dimeric structures). This approach predicted the ability of silibinin to directly bind the mouse and human STAT3 structures, with energy values ranging from −5.9 kcaL/mol to −8.5 kcaL/mol when using the mouse crystal structures 1BG1, 3CWG, 4E68, and from −5.6 kcaL/mol to −9.0 kcaL/mol when using the human homology models 1 and 2.

To add protein flexibility to the analysis and to better test the stability of the silibinin-STAT3 complexes, we carried out short MD simulations of 1 ns and applied MM/GBSA calculations to estimate more reliable binding energies, which are summarized in Table S4, S5, and S6. For MD simulations and MM/GBSA calculations, we selected mouse 4E68 and human homology model 1 to investigate the interactions with the SH2 domain, whereas mouse 1BG1 and human homology model 1 were selected to investigate the interactions with the DBD. Such approaches predicted the capacity of silibinin to bind mouse and human STAT3 structures with energy values ranging from −24.5797 kcaL/mol to −40.5752 kcaL/mol when using the mouse crystal structures 1BG1 and 4E68, and from −20.0086 kcaL/mol to −36.4145 kcaL/mol when using the human homology model 1.

3.4. Silibinin is predicted to bind to the SH2 and the DBD domains of STAT3

The binding modes of well-characterized direct STAT3i were significantly shared between the mouse PDB crystal structures and the human homology models, highlighting a high degree of conservation of the SH2 and DBD domains between mouse and human STAT3 proteins. The evaluation of the binding mode of silibinin to the monomeric form of the SH2 domain revealed a common group of predicted interacting residues shared with other direct STAT3i (Table S7); namely, M660, E638, K626, 7620, P639, V637, Y657, W623, and T714 in the mouse crystal structure 4E68, and S613, K626, P639, Q635, W623, and E638 in the human homology model 1. Silibinin was predicted not to share any interacting residue with S31-757 in the human homology model 1 of the monomeric form of the SH2 domain.

When evaluating the binding of silibinin to the dimeric form of the SH2 domain, we observed that silibinin was predicted to place differently to the remainder of the direct STAT3i (Table S8). Accordingly, silibinin was predicted to share with other direct STAT3 inhibitors a significant number of interacting residues in the human homology model 1 (K1658, M655, I1711, P1715, K709, V713, E652, V1713, L1666, I711, L666), but only a few interacting residues in the mouse crystal structure 4E68 (Q4644, E4638, and M648). Silibinin was predicted not to share any interacting residues with S31-M2001 and STX-0119 in the human homology model 1 of the dimeric form of the SH2 domain.

The evaluation of the binding mode of silibinin to the DBD revealed a common group of putative interacting residues shared with other

direct STAT3i (Table S9); namely, R423, K383, G419, R382, V432, and E415 in the mouse crystal structure 1BG1, and G419, G422, K383, G390, Q416, and R423 in the human homology model 1. Silibinin was predicted not to share any interacting residues with Stattic, S31-M2001, ln53–5418, S31-1757, and Compound 24 in the mouse crystal structure 1BG1, or S31-M2011, ln53-54A18, STX-0119, Compound 50, and Compound 24, in the human homology model 1.

3.5. The predicted binding mode of silibinin to STAT3 domains is different to other STAT3i

Silibinin was predicted to establish hydrogen bond interactions with S613, K626, E638, and M660 within the binding pocket of the monomeric SH2 domain of STAT3 (Fig. 4). Silibinin was predicted to additionally establish hydrophobic interactions with T620, W623, Q635, V637, E638, P639, Y657, and T714 (Fig. 4). The binding and putative inhibitory capacity of silibinin against the SH2 domain of STAT3 is underscored by the fact that it was predicted to share a significant number of interacting residues (W623, K626, Q635, V637, E638, Y657, and T714), or interact with those placed nearby or adjacent to those that were identified upon an extensive bibliographic search for key interacting residues employed by existing SH2-targeted STAT3i (F588, I589, S590, K591, E594, R595, R609, S611, E612, W623, K626, Q635, S636, V637, E638, Y657, I659, C687, Y705, T714, P715, T716, T717, and S727) (Fig. 4).

Silibinin was predicted to establish hydrogen bond interactions with S649, F710, and C722 (α chain), and T641 (β chain) within the binding pocket of the dimeric SH2 domains of STAT3 (Fig. 4). Silibinin was predicted to additionally establish hydrophobic interactions with M648, S649, L666, T708, F710, I711, and V713 (α chain) and with E638, P639, Y640, K658, I711, and V713 (β chain) (Fig. 4). Although most of these residues were placed nearby or adjacent to the above-mentioned key interacting residues employed by existing SH2-targeted STAT3 inhibitors (Supplementary Fig. S2), E638 was identified as the sole key interacting residue shared with silibinin, thus supporting the notion that direct STAT3i including silibinin might employ the binding pocket within the monomeric, but not the dimeric, SH2 domain of STAT3.

Silibinin was predicted to establish hydrogen bond interactions with R382, K383, G419, G422, R423, and G380 within the DBD of dimeric STAT3 (Fig. 4). Silibinin was predicted to additionally establish hydrophobic interactions with R382, K383, E415, R423, and V432. It should be noted that all these residues were included in the list of key interacting DBD residues that were identified upon an extensive bibliographic search of direct STAT3i; namely, Q326, P327, P330, M331, H332, K340, T341, V343, F345, T412, E415, N420, R423, I431, V432, S465, N466, I467, Q469, M470, W474, and N485. Moreover, despite the fact that DNA was complexed in the 1BG1 crystal structure for all the docking and MD simulations, silibinin was the sole STAT3i that was predicted to establish a hydrogen bond interaction with DT1005 (Fig. 4).

3.6. Silibinin prevents nuclear accumulation of activated STAT3

Since Y705 phosphorylation and dimerization of STAT3 is a prerequisite for its cytokine-induced nuclear translocation, we would expect a direct STAT3 SH2 domain inhibitor such as silibinin to inhibit IL-6-induced nuclear translocation of phospho-active STAT3. To test this, PC9 cells were seeded on coverslips and stimulated for 24 h with IL-6 in the absence or presence of silibinin. In untreated conditions, immunofluorescence microscopy showed that STAT3 was uniformly distributed between the cytoplasm and nucleus in PC9 cells; conversely, a greater number of STAT3 molecules appeared to be more prominently nuclear following IL-6 stimulation (Fig. 5A). The presence of silibinin failed to significantly alter the distribution pattern of total STAT3 in the absence of IL-6 stimulation; however, silibinin co-treatment suppressed IL-6-induced nuclear accumulation of STAT3. Moreover, when cells were stained for phosphorylated Y705 STAT3, we confirmed that IL-6-mediated nuclear accumulation of STAT3 is a molecular event largely dependent on the Y705 phosphorylation, which permits STAT3 to form dimers and enter the nuclei. Such IL-6-induced conspicuous STAT3 Y705 phosphorylation and translocation into the nucleus was completely prevented in the presence of silibinin (Fig. 5A).

3.7. Silibinin blocks transcriptional activity of STAT3

We then examined whether silibinin suppresses the transcriptional activity of STAT3 after IL-6 stimulation using a dual-luciferase assay system. HEK293 cells were transiently transfected with a reporter plasmid containing the STAT3-binding response element driving the expression of the luciferase gene. The STAT3-luciferase reporter construct responded exquisitely, in a dose-dependent manner, to graded concentrations of IL-6 (Fig. 5B). A concentration of silibinin as low as 100 μmoL/L completely prevented the transcriptional activity of STAT3 after stimulation with graded concentrations of IL-6. Moreover, when cells transiently transfected with the STAT3-luciferase reporter construct were stimulated with an optimal STAT3 activating concentration of IL-6 (50 ng/mL) in the presence of graded concentrations of silibinin, we confirmed the ability of silibinin to dramatically inhibit STAT3-dependent luciferase activity in a dose-dependent manner, with IC_{50} values lower than 25 μmoL/L (Fig. 5B).

3.8. Silibinin reduces the DNA binding activity of STAT3

Such a potent inhibitory effect of silibinin on the transcriptional activity of STAT3 might reflect not only its ability to influence tyrosine phosphorylation and nuclear accumulation of STAT3, but also the *in silico* predicted capability of silibinin to establish direct interactions with DNA in its inhibitory targeting to the DBD of STAT3. To evaluate the hypothesis that silibinin might also alter STAT3 retention via DNA binding, we employed the ELISA-based TransAM™ method to quantitatively evaluate the ability of the STAT3 residing in cellular nuclear extracts to bind its corresponding DNA consensus sequence (immobilized on the 96-well plate) when exposed to silibinin (Supplementary Fig. S1C). Nuclear extracts from IL-6-stimulated H460 and PC9 cells containing Y705-phosphorylated STAT3 were incubated with increasing concentrations of silibinin to directly determine the potency of silibinin to inhibit the DNA-binding activity of STAT3. A dose-dependent reduction in the DNA-binding activity of STAT3 was observed in the presence of silibinin (up to 60% at 200 μmoL/L silibinin; Fig. 6). When nuclear extracts obtained from H2228 cells, which exhibit constitutive activation of STAT3, were incubated in the presence of graded concentrations of silibinin, their STAT3 DNA binding activity was similarly reduced by up to 60% at 200 μmoL/L silibinin compared with vehicle-treated controls (Fig. 6).

4. Discussion

Although silibinin is known to be an inhibitor of STAT3 signaling, it remained to be clarified whether silibinin should be classified as an indirect STAT3i via kinase inhibition of the JAK/STAT pathway or as a direct STAT3i capable of binding and interfering with specific domains of the STAT3 protein. As with many other plant-derived secondary metabolites including cucurbitacin, curcumin, indirubin, cryptotanshinone, resveratrol, flavopiridol, and galiellalactone (Schust et al., 2006), silibinin has repeatedly been shown to inhibit STAT3 signaling in cancer cells (Jin et al., 2016; Bosch-Barrera and Menendez, 2015). While some of these natural products might operate as STAT3i through unknown targets, or have been shown to inhibit kinases upstream of STAT3 (JAK1/2, Src), others have been suggested to directly bind to STAT3 functional domains; for example, the SH2 domain, blocking STAT3 dimerization, or the STAT3 DBD, preventing sequence-specific

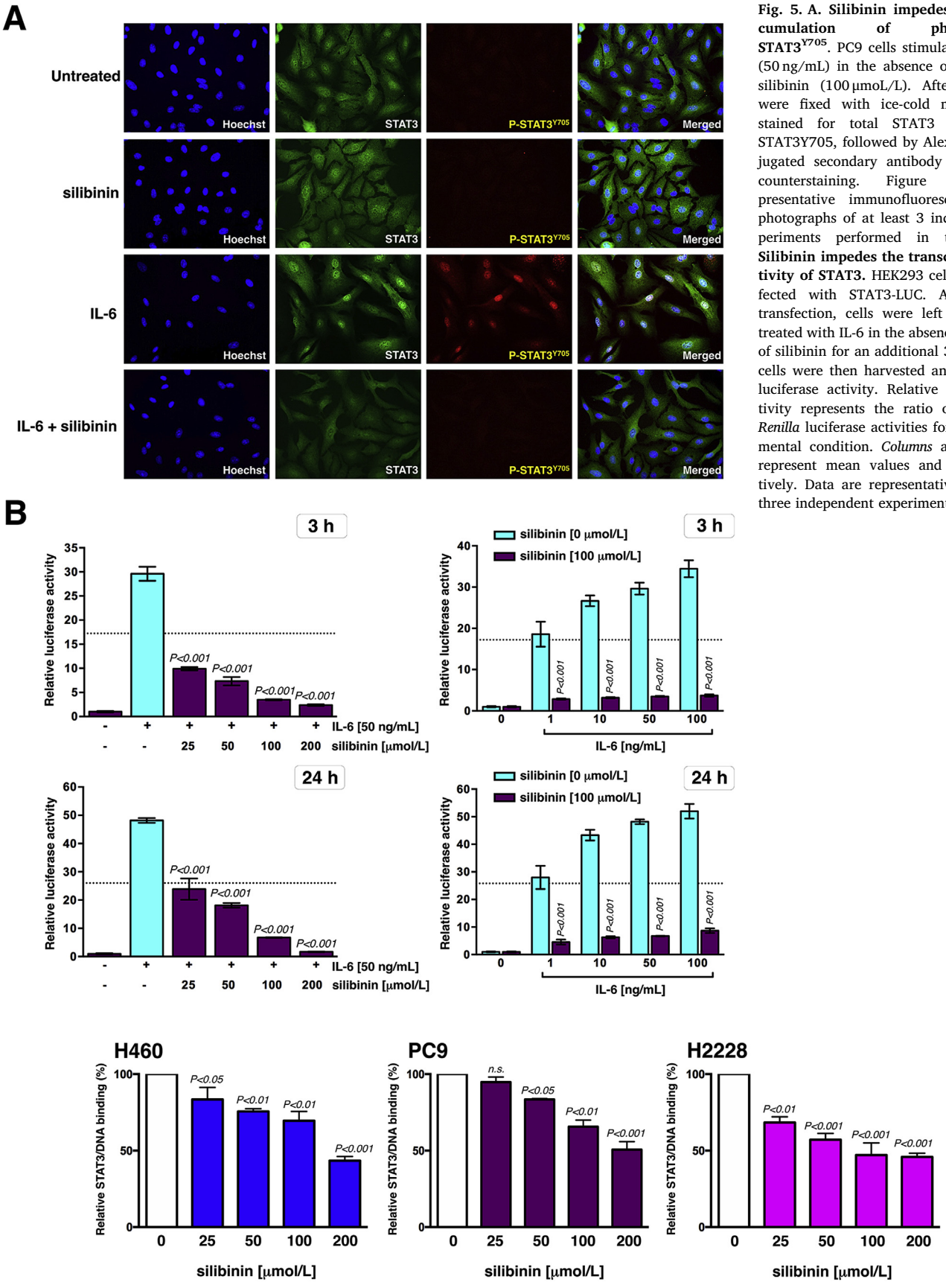

Fig. 5. A. Silibinin impedes nuclear accumulation of phospho-active STAT3^{Y705}. PC9 cells stimulated with IL-6 (50 ng/mL) in the absence or presence of silibinin (100 μmoL/L). After 24 h, cells were fixed with ice-cold methanol and stained for total STAT3 or phospho-STAT3Y705, followed by Alexa Fluor®-conjugated secondary antibody and Hoechst counterstaining. Figure shows representative immunofluorescence microphotographs of at least 3 independent experiments performed in triplicate. **B. Silibinin impedes the transcriptional activity of STAT3.** HEK293 cells were transfected with STAT3-LUC. At 24 h after transfection, cells were left untreated or treated with IL-6 in the absence or presence of silibinin for an additional 3 or 24 h. The cells were then harvested and assayed for luciferase activity. Relative luciferase activity represents the ratio of *Firefly* and *Renilla* luciferase activities for each experimental condition. *Columns* and *error bars* represent mean values and S.D., respectively. Data are representative of at least three independent experiments.

Fig. 6. Silibinin inhibits the DNA-binding activity of STAT3. The nuclear extracts from cells stimulated with IL-6 for 3 h were subjected to TransAM™ assays in microtitre wells coated with the STAT3 consensus sequence in the absence or presence of graded concentrations of silibinin for 3 h (see Supplementary Fig. S1C for schematic description of details concerning TransAM™ assays). *Columns* and *error bars* represent mean values and S.D., respectively. Data are representative of at least three independent experiments.

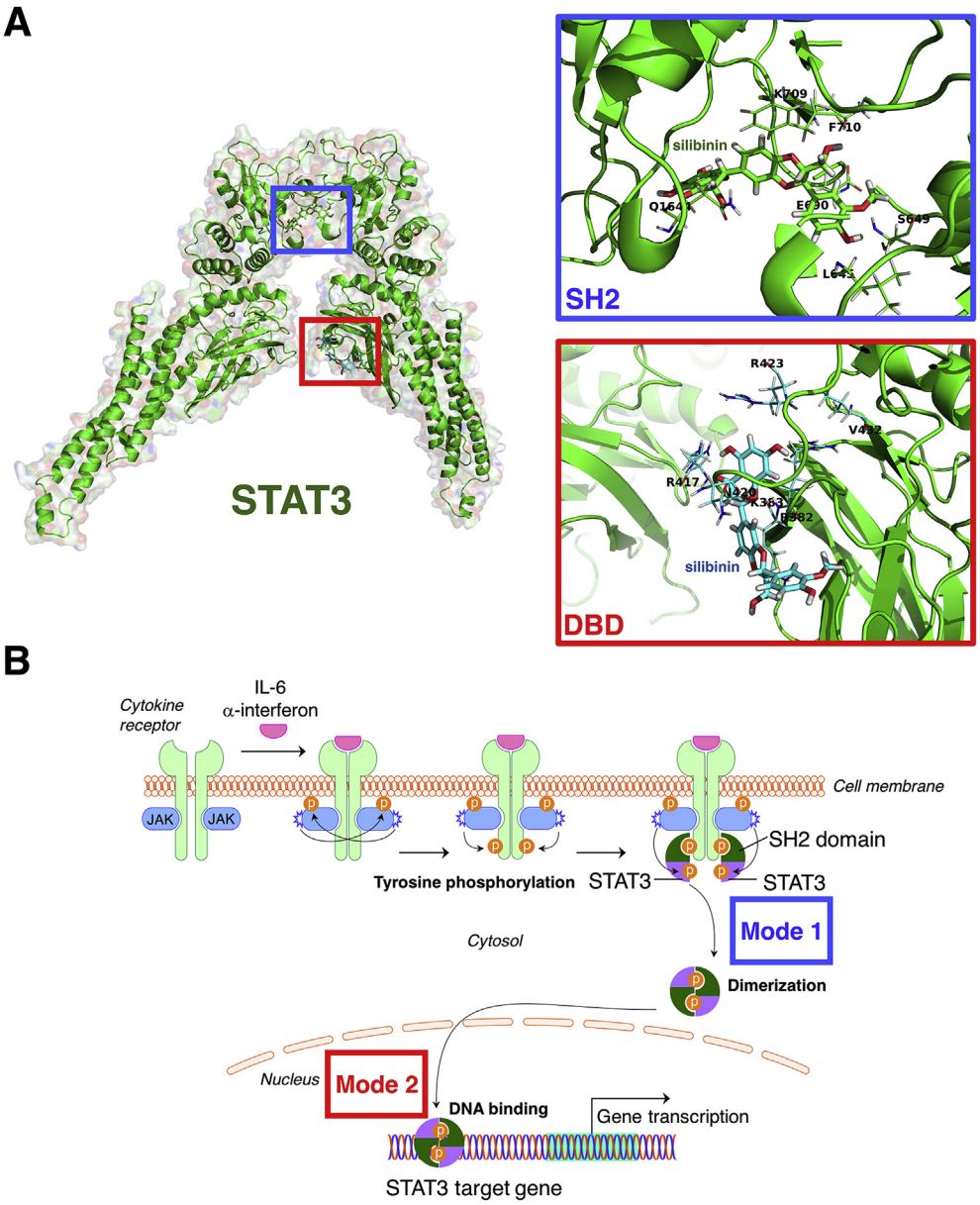

Fig. 7. Silibinin is a bimodal SH2- and DBD-targeted STAT3i. A. Global view of the STAT3 homodimer structure containing DNA (human homology model 2) and location of silibinin at the SH2 activation/dimerization and DNA-binding domains. **B.** Silibinin targeting of the SH2 domain of STAT3 monomers might prevent binding of STAT3 to activated cell surface receptors but also block dimerization (and subsequent trans-phosphorylation) of STAT3 molecules in the cytosol, thereby impeding nuclear accumulation of phospho-active STAT3. Silibinin additionally establishes direct interactions with DNA in its direct targeting of the DBD of STAT3, resulting in a significant inhibitory effect on STAT3-DNA binding. The bimodal SH2- and DBD-targeted behavior of silibinin might explain the proven therapeutic activity of silibinin in areas of unmet clinical need such as STAT3-dependent lung cancer and melanoma brain metastasis.

DNA binding ability and STAT3 transactivation activity. We now report that silibinin appears to work synergistically on STAT3 function through a bimodal mechanism of action involving blockade of the function of the STAT3 SH2 domain, which is crucial for both STAT3 activation and nuclear translocation, and of STAT3 transcriptional activity, which might involve not only disruption of STAT3 dimerization, but also a direct inhibition of the ability of STAT3 to bind DNA (Fig. 7A).

The STAT3 inhibitory activity of silibinin was not influenced by the pre-existing phosphorylation status of STAT3, as significant inhibitory effects were observed in cells with inducible, constitutive, and acquired phosphorylation at the Y705 site. LanthaScreen™-based cellular profiling assays revealed that silibinin attenuates the induced phospho-activation of Y705 in GFP-STAT3 genetic fusions without drastically altering the *in vitro* kinase activity of the STAT3 upstream kinases JAK1 and JAK2. Although these findings are consistent with the notion that silibinin exerts its pY705 STAT3 inhibitory effects by directly preventing the activating kinases from binding to the STAT3 SH2 domain, we acknowledge that further experimentation testing the direct effects of silibinin against other up-stream STAT3 kinases (e.g., SRC, ABL) and non-canonical STAT3 activators is needed before unambiguously concluding that silibinin exclusively operates as a direct STAT3i.

When we modeled the atomic details for the silibinin-driven inhibition of the activating phosphorylation Y705 on the SH2 domain, our first-in-class computational homology model of the human STAT3 protein allowing comparative docking and molecular dynamics simulation studies over fourteen different STAT3i, predicted that silibinin should molecularly behave as a direct STAT3i capable of establishing high-affinity interactions with the SH2 domain of STAT3. Using the binding site of the direct STAT3i OPB-31121, for which we dispose of detailed structural information explaining its inhibitory activity on the STAT3 SH2 domain (Brambilla et al., 2015), one could visualize the predicted ability of silibinin to interact with up to 60% of all the residues involved in the binding mode of a wide variety of structurally diverse STAT3i (Fig. 7A). The predicted ability of silibinin to bind the SH2 activation/dimerization domain therefore appears to rely on its capacity to overlap with the same cavity occupied by the majority of direct STAT3i to indirectly prevent Y705 phosphorylation in the monomeric SH2 domain of STAT3, but showing a unique binding mode.

Silibinin treatment is known to diminish nuclear DNA binding of

constitutively active STAT3 homodimers (Agarwal et al., 2007). Because Y705 phosphorylation is required for STAT3 to bind to specific DNA target sites but nuclear import of STAT3 takes place constitutively and independently of tyrosine phosphorylation (Liu et al., 2005; Reich and Liu, 2006), we employed immunofluorescence microscopy to visualize whether the *in silico* predicted ability of silibinin to operate as a direct STAT3i of the SH2 activation/dimerization domain translated into an altered intracellular localization of STAT3/phospho-active STAT3 *in cellulo*. The ability of silibinin to prevent the nuclear concentration of unphosphorylated STAT3 and Y705-phosphorylated STAT3 in response to IL-6 stimulation occurred without apparent accumulation of STAT3 in the cytoplasmic compartment. Although further work is needed to unambiguously exclude any indirect effect of silibinin in the importins-driven STAT3 trafficking to the nucleus (Liu et al., 2005; Cimica et al., 2011), our findings are compatible with a mechanism of action involving direct targeting of silibinin to the SH2 domain of STAT3 monomers, capable of preventing not only binding of STAT3 to activated cell surface receptors, but also to block dimerization (and subsequent trans-phosphorylation) of STAT3 molecules in the cytosol, thereby impeding nuclear accumulation of phospho-active STAT3.

To further evaluate the physiological role of silibinin on STAT3-mediated transactivation, we examined whether silibinin-driven changes in the sub-cellular accumulation of STAT3 correlated with changes in its transcriptional regulatory activity. Silibinin treatment was found to elicit the complete suppression of the IL-6-stimulated STAT3 transcriptional activity in living cells and, remarkably, such strong capability of silibinin to block STAT3-driven luciferase expression was evident even at concentrations that failed to completely shutdown the activating phosphorylation Y705 at the SH2 dimerization domain. Moreover, although *in vitro* experiments based on the detection of an STAT3 epitope that is accessible only when STAT3 is activated and bound to its DNA consensus binding site confirmed the *in silico* prediction of the capacity of silibinin to establish direct interactions with DNA in its targeting to the DBD of STAT3, once again the STAT3 DNA-binding inhibitory activity of silibinin took place at significantly higher concentrations than those needed to inhibit STAT3-driven transcriptional activity. Because parallel immunoblotting experiments with IL-6-stimulated nuclear extracts showed that silibinin can block the binding of activated STAT3 to its consensus DNA sequence in isolated nuclear extracts without altering the phosphorylation status of Y705 (data not shown), these findings altogether suggest that the ability of silibinin to inhibit STAT3-directed transcription in living cells does not rely exclusively on the SH2 domain-related inhibition of STAT3 dimerization in the cytosol, but also involves direct inhibition of STAT3 via binding to the DBD regardless of the STAT3 dimerization status. Nevertheless, the unique behavior of silibinin as a bimodal SH2- and DBD-STAT3i that strongly disrupts STAT3 transcriptional activity is definitively supported by the fact that cells engineered to overexpress a constitutively active form of STAT3 (Bromberg et al., 1999), which dimerizes spontaneously, binds to DNA and activates transcription, remain largely unresponsive to the inhibitory effects of silibinin in key transcriptional targets of STAT3 (Shukla et al., 2015; Priego et al., 2018). The so-called STAT3C mutant, in which the SH2 domain A661 and N663 residues are substituted with cysteine residues allowing a disulfide bond to form between two unphosphorylated STAT3 monomers, still requires Y705 phosphorylation for functional activation via promotion of maximal DNA binding affinity, slower off-rate, and protection from inactivation from phosphatases, resulting in the accumulation of transcriptionally active STAT3 dimer complexes (Liddle et al., 2006). We recently reported that the decreased ability of silibinin to bind the STAT3C mutant translates into refractoriness of STAT3C-expressing cells to silibinin (Priego et al., 2018), demonstrating the STAT3-dependency on the phenotypic effects of silibinin.

Beyond common issues in the development of other anti-cancer drug families such as rapid degradation, lack of cell penetrance or lack of binding specificity, the observation that inhibition of active STAT3 dimers alone via targeting to the SH2 domain may not be sufficient in efficaciously preventing STAT3 activity (Huang et al., 2016) together with the preliminary support to the notion that targeting the DBD may prove more efficient in abrogating STAT3 activity than targeting the SH2 domain in cellular systems (Furtek et al., 2016b), can largely explain why the majority of direct STAT3i have yet to enter clinical evaluation. We have recently reported that silibinin-driven STAT3 blocking translates into proven therapeutic activity in areas of unmet clinical need such as lung cancer and melanoma brain metastasis, which portend a poor prognosis and have few therapeutic options (Bosch-Barrera et al., 2016; Priego et al., 2018). We now report the unique characteristics of silibinin as a promising lead of a new generation of bimodal SH2- and DBD-targeting STAT3i (Fig. 7B) that may transform the clinical management of secondary brain tumors.

5. Conclusion

To the best of our knowledge, this is the first report establishing that the flavonolignan silibinin is a novel direct STAT3i. Our systematic approach performed at multiple levels of integration including *in vitro*, *in silico* computational modeling, and *in cellulo* experimentation, demonstrates that: a.) silibinin could directly bind the SH2 domain of STAT3 to prevent Y705 phosphorylation-related STAT3 activation and dimerization; b.) silibinin could establish direct interactions with DNA in its targeting to the STAT3 DNA-binding domain (DBD); and c.) silibinin impedes the activation, dimerization, nuclear translocation, DNA-binding, and transcriptional activity of STAT3. Our findings showing the unique features and putative direct modes of action of silibinin against STAT3 will be highly relevant for further development and design of new, more effective silibinin-based STAT3i.

Conflicts of interest

L.L-P, A. N-C, and M. S-M are employees of Mind the Byte S.L. All other authors have no competing interests to declare.

Acknowledgments

This work was supported by grants from the Ministerio de Ciencia e Innovación (Grant SAF2016-80639-P to J. A. Menendez), Plan Nacional de I + D + I, Spain, and the Agència de Gestió d'Ajuts Universitaris i de Recerca (AGAUR) (Grant 2014 SGR229 to J. A. Menendez). This study was supported also by unrestricted research grants from Roche Pharma (Spain) and Astellas Pharma (Spain) to the Program Against Cancer Therapeutic Resistance (ProCURE, Catalan Institute of Oncology). Joaquim Bosch-Barrera is supported by SEOM, Pfizer (Grant WI190764), Boehringer Ingelheim, Meda Pharma, and Pla strategic de recerca i innovació en salut 2016–2020 de la Generalitat de Catalunya (SLT006/17/114). Elisabet Cuyàs is supported by a Sara Borrell post-doctoral contract (CD15/00033) from the Ministerio de Sanidad y Consumo, Fondo de Investigación Sanitaria (FIS), Spain. The authors would like to thank Dr. Kenneth McCreath for editorial support.

Appendix A. Supplementary data

Supplementary data related to this article can be found at http://dx.doi.org/10.1016/j.fct.2018.04.028.

Transparency document

Transparency document related to this article can be found online at http://dx.doi.org/10.1016/j.fct.2018.04.028.

References

Agarwal, C., Tyagi, A., Kaur, M., Agarwal, R., 2007. Silibinin inhibits constitutive activation of Stat3, and causes caspase activation and apoptotic death of human prostate carcinoma DU145 cells. Carcinogenesis 28, 1463–1470. https://doi.org/10.1093/carcin/bgm042.

Agarwal, R., Agarwal, C., Ichikawa, H., Singh, R.P., Aggarwal, B.B., 2006. Anticancer potential of silymarin: from bench to bed side. Anticancer Res. 26, 4457–4498.

Ali, A.M., Gómez-Biagi, R.F., Rosa, D.A., Lai, P.-S., Heaton, W.L., Park, J.S., Eiring, A.M., Vellore, N.A., de Araujo, E.D., Ball, D.P., Shouksmith, A.E., Patel, A.B., Deininger, M.W., O'Hare, T., Gunning, P.T., 2016. Disarming an electrophilic warhead: retaining potency in tyrosine kinase inhibitor (TKI)-Resistant CML lines while circumventing pharmacokinetic liabilities. ChemMedChem 11, 850–861. https://doi.org/10.1002/cmdc.201600021.

Becker, S., Groner, B., Muller, C.W., 1998. Three-dimensional structure of the Stat3beta homodimer bound to DNA. Nature 394, 145–151. https://doi.org/10.1038/28101.

Bosch-Barrera, J., Corominas-Faja, B., Cuyàs, E., Martin-Castillo, B., Brunet, J., Menendez, J.A., 2014. Silibinin administration improves hepatic failure due to extensive liver infiltration in a breast cancer patient. Anticancer Res. 34, 4323–4328.

Bosch-Barrera, J., Menendez, J.A., 2015. Silibinin and STAT3: a natural way of targeting transcription factors for cancer therapy. Canc. Treat Rev. 41, 540–546. https://doi.org/10.1016/j.ctrv.2015.04.008.

Bosch-Barrera, J., Queralt, B., Menendez, J.A., 2017. Targeting STAT3 with silibinin to improve cancer therapeutics. Canc. Treat Rev. 58, 61–69. https://doi.org/10.1016/j.ctrv.2017.06.003.

Bosch-Barrera, J., Sais, E., Cañete, N., Marruecos, J., Cuyàs, E., Izquierdo, A., Porta, R., Haro, M., Brunet, J., Pedraza, S., Menendez, J.A., 2016. Response of brain metastasis from lung cancer patients to an oral nutraceutical product containing silibinin. Oncotarget 7, 32006–32014. https://doi.org/10.18632/oncotarget.7900.

Brambilla, L., Genini, D., Laurini, E., Merulla, J., Perez, L., Fermeglia, M., Carbone, G.M., Pricl, S., Catapano, C.V., 2015. Hitting the right spot: mechanism of action of OPB-31121, a novel and potent inhibitor of the Signal Transducer and Activator of Transcription 3 (STAT3). Mol. Oncol 9, 1194–1206. https://doi.org/10.1016/j.molonc.2015.02.012.

Bromberg, J.F., Wrzeszczynska, M.H., Devgan, G., Zhao, Y., Pestell, R.G., Albanese, C., Darnell, J.E., 1999. Stat3 as an oncogene. Cell 98, 295–303. https://doi.org/10.1016/S0092-8674(00)81959-5.

Chang, Q., Bournazou, E., Sansone, P., Berishaj, M., Gao, S.P., Daly, L., Wels, J., Theilen, T., Granitto, S., Zhang, X., Cotari, J., Alpaugh, M.L., de Stanchina, E., Manova, K., Li, M., Bonafe, M., Ceccarelli, C., Taffurelli, M., Santini, D., Altan-Bonnet, G., Kaplan, R., Norton, L., Nishimoto, N., Huszar, D., Lyden, D., Bromberg, J., 2013. The IL-6/JAK/Stat3 feed-forward loop drives tumorigenesis and metastasis. Neoplasia 15, 848–862.

Chen, Y., Wang, J., Wang, X., Liu, X., Li, H., Lv, Q., Zhu, J., Wei, B., Tang, Y., 2013. STAT3, a poor survival predicator, Is associated with lymph node metastasis from breast cancer. J. Breast Cancer 16, 40–49. https://doi.org/10.4048/jbc.2013.16.1.40.

Chittezhath, M., Deep, G., Singh, R.P., Agarwal, C., Agarwal, R., 2008. Silibinin inhibits cytokine-induced signaling cascades and down-regulates inducible nitric oxide synthase in human lung carcinoma A549 cells. Mol. Canc. Therapeut. 7, 1817–1826. https://doi.org/10.1158/1535-7163.MCT-08-0256.

Cimica, V., Chen, H.-C., Iyer, J.K., Reich, N.C., 2011. Dynamics of the STAT3 transcription factor: nuclear import dependent on Ran and importin-β1. PLoS One 6, e20188. https://doi.org/10.1371/journal.pone.0020188.

Cufí, S., Bonavia, R., Vazquez-Martin, A., Corominas-Faja, B., Oliveras-Ferraros, C., Cuyàs, E., Martin-Castillo, B., Barrajón-Catalán, E., Visa, J., Segura-Carretero, A., Bosch-Barrera, J., Joven, J., Micol, V., Menendez, J.A., 2013a. Silibinin meglumine, a water-soluble form of milk thistle silymarin, is an orally active anti-cancer agent that impedes the epithelial-to-mesenchymal transition (EMT) in EGFR-mutant non-small-cell lung carcinoma cells. Food Chem. Toxicol. 60, 360–368. https://doi.org/10.1016/j.fct.2013.07.063.

Cufí, S., Bonavia, R., Vazquez-Martin, A., Oliveras-Ferraros, C., Corominas-Faja, B., Cuyàs, E., Martin-Castillo, B., Barrajón-Catalán, E., Visa, J., Segura-Carretero, A., Joven, J., Bosch-Barrera, J., Micol, V., Menendez, J.A., 2013b. Silibinin suppresses EMT-driven erlotinib resistance by reversing the high miR-21/low miR-200c signature in vivo. Sci. Rep. 3, 2459. https://doi.org/10.1038/srep02459.

Cuyàs, E., Pérez-Sánchez, A., Micol, V., Menendez, J.A., Bosch-Barrera, J., 2016. STAT3-targeted treatment with silibinin overcomes the acquired resistance to crizotinib in ALK-rearranged lung cancer. Cell Cycle 1–6. https://doi.org/10.1080/15384101.2016.1245249.

Eiring, A.M., Page, B.D.G., Kraft, I.L., Mason, C.C., Vellore, N.A., Resetca, D., Zabriskie, M.S., Zhang, T.Y., Khorashad, J.S., Engar, A.J., Reynolds, K.R., Anderson, D.J., Senina, A., Pomicter, A.D., Arpin, C.C., Ahmad, S., Heaton, W.L., Tantravahi, S.K., Todic, A., Colaguori, R., Moriggl, R., Wilson, D.J., Baron, R., O'Hare, T., Gunning, P.T., Deininger, M.W., 2015. Combined STAT3 and BCR-ABL1 inhibition induces synthetic lethality in therapy-resistant chronic myeloid leukemia. Leukemia 29, 586–597. https://doi.org/10.1038/leu.2014.245.

Fagard, R., Metelev, V., Souissi, I., Baran-Marszak, F., 2013. STAT3 inhibitors for cancer therapy: have all roads been explored? JAK-STAT 2, e22882. https://doi.org/10.4161/jkst.22882.

Flaig, T.W., Glodé, M., Gustafson, D., Van Bokhoven, A., Tao, Y., Wilson, S., Su, L.J., Li, Y., Harrison, G., Agarwal, R., Crawford, E.D., Lucia, M.S., Pollak, M., 2010. A study of high-dose oral silybin-phytosome followed by prostatectomy in patients with localized prostate cancer. Prostate 70, 848–855. https://doi.org/10.1002/pros.21118.

Furqan, M., Akinleye, A., Mukhi, N., Mittal, V., Chen, Y., Liu, D., 2013. STAT inhibitors for cancer therapy. J. Hematol. Oncol. 6, 90. https://doi.org/10.1186/1756-8722-6-90.

Furtek, S.L., Backos, D.S., Matheson, C.J., Reigan, P., 2016a. Strategies and approaches of targeting STAT3 for cancer treatment. ACS Chem. Biol. 11, 308–318. https://doi.org/10.1021/acschembio.5b00945.

Furtek, S.L., Matheson, C.J., Backos, D.S., Reigan, P., 2016b. Evaluation of quantitative assays for the identification of direct signal transducer and activator of transcription 3 (STAT3) inhibitors. Oncotarget 7, 77998–78008. https://doi.org/10.18632/oncotarget.12868.

Gažák, R., Walterová, D., Křen, V., 2007. Silybin and silymarin–new and emerging applications in medicine. Curr. Med. Chem. 14, 315–338. https://doi.org/10.2174/092986707779941159.

Hoh, C., Boocock, D., Marczylo, T., Singh, R., Berry, D.P., Dennison, A.R., Hemingway, D., Miller, A., West, K., Euden, S., Garcea, G., Farmer, P.B., Steward, W.P., Gescher, A.J., 2006. Pilot study of oral silibinin, a putative chemopreventive agent, in colorectal cancer patients: silibinin levels in plasma, colorectum, and liver and their pharmacodynamic consequences. Clin. Canc. Res. 12, 2944–2950. https://doi.org/10.1158/1078-0432.CCR-05-2724.

Huang, W., Dong, Z., Chen, Y., Wang, F., Wang, C.J., Peng, H., He, Y., Hangoc, G., Pollok, K., Sandusky, G., Fu, X.-Y., Broxmeyer, H.E., Zhang, Z.-Y., Liu, J.-Y., Zhang, J.-T., 2016. Small-molecule inhibitors targeting the DNA-binding domain of STAT3 suppress tumor growth, metastasis and STAT3 target gene expression in vivo. Oncogene 35, 783–792. https://doi.org/10.1038/onc.2015.215.

Jin, Y., Kim, Y., Lee, Y.-J., Han, D.C., K.B, M., 2016. Natural products targeting STAT3 signaling pathways in cancer cells. Biodesign 4, 1–17.

Kroon, P., Berry, P.A., Stower, M.J., Rodrigues, G., Mann, V.M., Simms, M., Bhasin, D., Chettiar, S., Li, C., Li, P.K., Maitland, N.J., Collins, A.T., 2013. JAK-STAT blockade inhibits tumor initiation and clonogenic recovery of prostate cancer stem-like cells. Canc. Res. 73, 5288–5298. https://doi.org/10.1158/0008-5472.CAN-13-0874.

Lai, P.-S., Rosa, D.A., Magdy Ali, A., Gómez-Biagi, R.F., Ball, D.P., Shouksmith, A.E., Gunning, P.T., 2015. A STAT inhibitor patent review: progress since 2011. Expert Opin. Ther. Pat. 25, 1397–1421. https://doi.org/10.1517/13543776.2015.1086749.

Lee, H.-J., Zhuang, G., Cao, Y., Du, P., Kim, H.-J., Settleman, J., 2014. Drug resistance via feedback activation of Stat3 in oncogene-addicted cancer cells. Canc. Cell 26, 207–221. https://doi.org/10.1016/j.ccr.2014.05.019.

Liddle, F.J., Alvarez, J.V., Poli, V., Frank, D.A., 2006. Tyrosine phosphorylation is required for functional activation of disulfide-containing constitutively active STAT mutants. Biochemistry 45, 5599–5605. https://doi.org/10.1021/bi0525674.

Lin, L., Hutzen, B., Li, P.-K., Ball, S., Zuo, M., DeAngelis, S., Foust, E., Sobo, M., Friedman, L., Bhasin, D., Cen, L., Li, C., Lin, J., 2010. A novel small molecule, LLL12, inhibits STAT3 phosphorylation and activities and exhibits potent growth-suppressive activity in human cancer cells. Neoplasia 12, 39–50.

Liu, L., McBride, K.M., Reich, N.C., 2005. STAT3 nuclear import is independent of tyrosine phosphorylation and mediated by importin- 3. Proc. Natl. Acad. Sci. Unit. States Am. 102, 8150–8155. https://doi.org/10.1073/pnas.0501643102.

Liu, X., He, Z., Li, C.-H., Huang, G., Ding, C., Liu, H., 2012. Correlation analysis of JAK-STAT pathway components on prognosis of patients with prostate cancer. Pathol. Oncol. Res. 18, 17–23. https://doi.org/10.1007/s12253-011-9410-y.

Mao, X., Ren, Z., Parker, G.N., Sondermann, H., Pastorello, M.A., Wang, W., McMurray, J.S., Demeler, B., Darnell, J.E., Chen, X., 2005. Structural bases of unphosphorylated STAT1 association and receptor binding. Mol. Cell 17, 761–771. https://doi.org/10.1016/j.molcel.2005.02.021.

Matsuno, K., Masuda, Y., Uehara, Y., Sato, H., Muroya, A., Takahashi, O., Yokotagawa, T., Furuya, T., Okawara, T., Otsuka, M., Ogo, N., Ashizawa, T., Oshita, C., Tai, S., Ishii, H., Akiyama, Y., Asai, A., 2010. Identification of a new series of STAT3 inhibitors by virtual screening. ACS Med. Chem. Lett. 1, 371–375. https://doi.org/10.1021/ml1000273.

Miklossy, G., Hilliard, T.S., Turkson, J., 2013. Therapeutic modulators of STAT signalling for human diseases. Nat. Rev. Drug Discov. 12, 611–629. https://doi.org/10.1038/nrd4088.

Misra, S.K., De, A., Pan, D., 2018. Targeted delivery of STAT-3 modulator to breast cancer stem-like cells downregulates a series of stemness genes. Mol. Canc. Therapeut. 17, 119–129. https://doi.org/10.1158/1535-7163.MCT-17-0070.

Nan, J., Du, Y., Chen, X., Bai, Q., Wang, Y., Zhang, X., Zhu, N., Zhang, J., Hou, J., Wang, Q., Yang, J., 2014. TPCA-1 is a direct dual inhibitor of STAT3 and NF-κb and regresses mutant EGFR-associated human non-small cell lung cancers. Mol. Canc. Therapeut. 13, 617–629. https://doi.org/10.1158/1535-7163.MCT-13-0464.

Nkansah, E., Shah, R., Collie, G.W., Parkinson, G.N., Palmer, J., Rahman, K.M., Bui, T.T., Drake, A.F., Husby, J., Neidle, S., Zinzalla, G., Thurston, D.E., Wilderspin, A.F., 2013. Observation of unphosphorylated STAT3 core protein binding to target dsDNA by PEMSA and X-ray crystallography. FEBS Lett. 587, 833–839. https://doi.org/10.1016/j.febslet.2013.01.065.

Poli, V., Camporeale, A., 2015. STAT3-Mediated metabolic reprograming in cellular transformation and implications for drug resistance. Front. Oncol 5 (121). https://doi.org/10.3389/fonc.2015.00121.

Priego, N., Zhu, L., Monteiro, C., Mulders, M., Wasilewski, D., Bindeman, W., Doglio, L., Martínez, L., Martínez-Saez, E., Ramón y Cajal, S., Megías, D., Hernández-Encinas, E., Blanco-Aparicio, C., Martínez, L., Zarzuela, E., Muñoz, J., Fustero-Torres, C., Pineiro, E., Hernández-Laín, A., Bertero, L., Poli, V., Sánchez-Martínez, M., Menendez, J.A., Soffietti, R., Bosch-Barrera, J., Valiente, V., 2018. STAT3 labels a subpopulation of reactive astrocytes required for brain metastasis. Nat. Med (in press).

Rath, K.S., Naidu, S.K., Lata, P., Bid, H.K., Rivera, B.K., McCann, G.A., Tierney, B.J., ElNaggar, A.C., Bravo, V., Leone, G., Houghton, P., Hideg, K., Kuppusamy, P., Cohn, D.E., Selvendiran, K., 2014. HO-3867, a safe STAT3 inhibitor, is selectively cytotoxic to ovarian cancer. Canc. Res. 74, 2316–2327. https://doi.org/10.1158/0008-5472.CAN-13-2433.

Reich, N.C., Liu, L., 2006. Tracking STAT nuclear traffic. Nat. Rev. Immunol. 6, 602–612.

https://doi.org/10.1038/nri1885.
Ren, Z., Mao, X., Mertens, C., Krishnaraj, R., Qin, J., Mandal, P.K., Romanowski, M.J., McMurray, J.S., Chen, X., 2008. Crystal structure of unphosphorylated STAT3 core fragment. Biochem. Biophys. Res. Commun. 374, 1–5. https://doi.org/10.1016/j.bbrc.2008.04.049.
Sansone, P., Bromberg, J., 2012. Targeting the interleukin-6/jak/stat pathway in human malignancies. J. Clin. Oncol. 30, 1005–1014. https://doi.org/10.1200/JCO.2010.31.8907.
Schroeder, A., Herrmann, A., Cherryholmes, G., Kowolik, C., Buettner, R., Pal, S., Yu, H., Müller-Newen, G., Jove, R., 2014. Loss of androgen receptor expression promotes a stem-like cell phenotype in prostate cancer through STAT3 signaling. Canc. Res. 74, 1227–1237. https://doi.org/10.1158/0008-5472.CAN-13-0594.
Schust, J., Sperl, B., Hollis, A., Mayer, T.U., Berg, T., 2006. Stattic: a small-molecule inhibitor of STAT3 activation and dimerization. Chem. Biol. 13, 1235–1242. https://doi.org/10.1016/j.chembiol.2006.09.018.
Shahani, V.M., Yue, P., Fletcher, S., Sharmeen, S., Sukhai, M.A., Luu, D.P., Zhang, X., Sun, H., Zhao, W., Schimmer, A.D., Turkson, J., Gunning, P.T., 2011. Design, synthesis, and in vitro characterization of novel hybrid peptidomimetic inhibitors of STAT3 protein. Bioorg. Med. Chem. 19, 1823–1838. https://doi.org/10.1016/j.bmc.2010.12.010.
Shukla, S.K., Dasgupta, A., Mehla, K., Gunda, V., Vernucci, E., Souchek, J., Goode, G., King, R., Mishra, A., Rai, I., Nagarajan, S., Chaika, N.V., Yu, F., Singh, P.K., 2015. Silibinin-mediated metabolic reprogramming attenuates pancreatic cancer-induced cachexia and tumor growth. Oncotarget 6, 41146–41161. https://doi.org/10.18632/oncotarget.5843.
Siegel, A.B., Narayan, R., Rodriguez, R., Goyal, A., Jacobson, J.S., Kelly, K., Ladas, E., Lunghofer, P.J., Hansen, R.J., Gustafson, D.L., Flaig, T.W., Yann Tsai, W., Wu, D.P.H., Lee, V., Greenlee, H., 2014. A phase I dose-finding study of silybin phosphatidylcholine (milk thistle) in patients with advanced hepatocellular carcinoma. Integr. Canc. Ther. 13, 46–53. https://doi.org/10.1177/1534735413490798.
Singh, R.P., Raina, K., Deep, G., Chan, D., Agarwal, R., 2009. Silibinin suppresses growth of human prostate carcinoma PC-3 orthotopic xenograft via activation of extracellular signal-regulated kinase 1/2 and inhibition of signal transducers and activators of transcription signaling. Clin. Canc. Res. 15, 613–621. https://doi.org/10.1158/1078-0432.CCR-08-1846.
Siveen, K.S., Sikka, S., Surana, R., Dai, X., Zhang, J., Kumar, A.P., Tan, B.K.H., Sethi, G., Bishayee, A., 2014. Targeting the STAT3 signaling pathway in cancer: role of synthetic and natural inhibitors. Biochim. Biophys. Acta Rev. Canc 1845, 136–154. https://doi.org/10.1016/j.bbcan.2013.12.005.
Tan, F.H., Putoczki, T.L., Stylli, S.S., Luwor, R.B., 2014. The role of STAT3 signaling in mediating tumor resistance to cancer therapy. Curr. Drug Targets 15, 1341–1353. https://doi.org/10.2174/1389450115666141120104146.
Timofeeva, O.A., Chasovskikh, S., Lonskaya, I., Tarasova, N.I., Khavrutskii, L., Tarasov, S.G., Zhang, X., Korostyshevskiy, V.R., Cheema, A., Zhang, L., Dakshanamurthy, S., Brown, M.L., Dritschilo, A., 2012. Mechanisms of unphosphorylated STAT3 transcription factor binding to DNA. J. Biol. Chem. 287, 14192–14200. https://doi.org/10.1074/jbc.M111.323899.
Tong, M., Wang, J., Jiang, N., Pan, H., Li, D., 2017. Correlation between p-STAT3 overexpression and prognosis in lung cancer: a systematic review and meta-analysis. PLoS One 12. https://doi.org/10.1371/journal.pone.0182282.
Wang, T., Fahrmann, J.F., Lee, H., Li, Y.-J., Tripathi, S.C., Yue, C., Zhang, C., Lifshitz, V., Song, J., Yuan, Y., Somlo, G., Jandial, R., Ann, D., Hanash, S., Jove, R., Yu, H., 2018. JAK/STAT3-Regulated fatty acid β-oxidation is critical for breast cancer stem cell self-renewal and chemoresistance. Cell Metabol. 27, 136–150. e5. https://doi.org/10.1016/j.cmet.2017.11.001.
Wu, P., Wu, D., Zhao, L., Huang, L., Shen, G., Huang, J., Chai, Y., 2016. Prognostic role of STAT3 in solid tumors: a systematic review and meta-analysis. Oncotarget 7, 19863–19883. https://doi.org/ https://doi.org/10.18632/oncotarget.7887.
Yu, H., Lee, H., Herrmann, A., Buettner, R., Jove, R., 2014. Revisiting STAT3 signalling in cancer: new and unexpected biological functions. Nat. Rev. Canc. 14, 736–746. https://doi.org/10.1038/nrc3818.
Yu, H., Pardoll, D., Jove, R., 2009. STATs in cancer inflammation and immunity: a leading role for STAT3. Nat. Rev. Canc. 9, 798–809. https://doi.org/10.1038/nrc2734.
Yue, P., Turkson, J., 2009. Targeting STAT3 in cancer: how successful are we? Expert Opin. Investig. Drugs 18, 45–56. https://doi.org/10.1517/13543780802565791.
Zhang, X., Sun, Y., Pireddu, R., Yang, H., Urlam, M.K., Lawrence, H.R., Guida, W.C., Lawrence, N.J., Sebti, S.M., 2013. A novel inhibitor of STAT3 homodimerization selectively suppresses STAT3 activity and malignant transformation. Canc. Res. 73, 1922–1933. https://doi.org/10.1158/0008-5472.CAN-12-3175.
Zhao, C., Li, H., Lin, H.J., Yang, S., Lin, J., Liang, G., 2016. Feedback activation of STAT3 as a cancer drug-resistance mechanism. Trends Pharmacol. Sci. 37, 47–61. https://doi.org/10.1016/j.tips.2015.10.001.